# Online Detection of Fundamental and Interharmonics in AC Mains for Parallel Operation of Multiple Grid-Connected Power Converters

Boli Chen, Gilberto Pin, Wai Man Ng, *Member, IEEE*, Peng Li, Thomas Parisini, *Fellow, IEEE,* and Shu-Yuen Ron Hui, *Fellow, IEEE*

***Abstract*— Parallel operation of multiple grid-connected power converters through LCL filters is known to have the potential problem of triggering oscillations in the ac mains. Such oscillatory frequencies are not integral multiples of the fundamental frequency and hence form a new source of interharmonics. Early detection of such oscillations is essential for the parallel power converters to move out of the unstable zone. This paper presents an online observer-based algorithm that can perform fast detection of interharmonics within a specified frequency band. The algorithm has been adopted in a specific and reduced form from an integral observer algorithm for detection of fundamental and interharmonic voltage components in the ac mains. A new method based on the kernel signal for fast interharmonic detection is proposed and practically verified. It has been implemented in a digital controller to detect oscillations such as those occurring between two grid-connected power converters. The practical results indicate that the algorithm can locate such frequency within the specific frequency band within 1 mains cycle.**

***Index Terms*— fundamental extraction, harmonics detection, interharmonics detection, active power filters**

## I. Introduction

The tsunami and the subsequent disaster in Fukushima nuclear power facilities in March 2011 have prompted some countries such as Germany to speed up the deployment of distributed renewable energy sources such as wind and solar energy. On the domestic level, rooftop photovoltaic (PV) systems have been increasingly installed in the distribution networks. Unlike traditional fossil-fuel based power generation, distributed renewable generation systems are usually bidirectional. For example, solar power generated by the PV systems can be consumed by domestic loads, while surplus power can be injected into the power supply side (i.e. the distribution networks).

Renewable energy sources are connected to the distribution networks through power electronics circuits such as bi-directional power inverters [1]. Grid-connected inverters are usually connected to the ac mains through LCL filters [2]. Increasing use of grid-connected PV inverters pose new technical challenges. Reports over the last two decades indicate that parallel operations of multiple grid-connected inverters could trigger resonance among their LCL filters [3]-[7]. Such resonance could result in not only voltage oscillations in the ac mains, but also system instability because the grid-connected inverter requires the mains voltage waveform for synchronization in the control loop. Recently, the resonance characteristics and stability problem caused by the interactions of multiple parallel LCL-filtered inverters has been reported in [8]. If resonance occurs, the control systems of the parallel power inverters should move their operating points out of the unstable zones. An alternative approach is to use active damping circuits to damp down the oscillations [9], [10].

Because grid-connected power inverters are power electronics circuits that require the information of the mains voltage, early and fast detection of such resonance is paramount in stability control of the parallel inverters. The challenge in this project lies with the nature of this type of oscillations, because the LCL filter parameters may vary from one manufacturer to another. The oscillatory frequencies are not identical in all situations and these frequencies are not integral numbers of the fundamental frequency. In other words, these oscillatory voltage components are ‘interharmonics”. Such interharmonics tend to fall within a certain frequency band that depends on the switching frequency of the inverters and the parameters of the LCL filters. In [11] and [12], the interharmonics are in the range of about 1.7 kHz to 2.0 kHz.

The presence of interharmonics makes it difficult to model and detect the frequency components in the power system signals [26]. Conventionally, the discrete Fourier transform (DFT) and its many variants [15]-[19] are preferred for the efficiency in stationary conditions (i.e., when the frequency content is constant within the considered time-window) and for their computational efficiency. In [14], the DFT is expressed in a matrix-vector formulation leading to

Manuscript received April 6 2017; revised May 19 2017 and Septempter 6 2017 accepted December 11 2017 6 2016. This work was supported in part by the Hong Kong Research Council under the Theme-based Research Fund T23-701/14-N.

Boli Chen is with the Department of Electrical & Electronic Engineering, Imperial College London (e-mail: boli.chen10@imperial.ac.uk).

G. Pin is with Electrolux, Italy (e-mail: gilbertopin@alice.it).

W.M. Ng is with the Department of Electrical & Electronic Engineering, The University of Hong Kong (e-mail: wmng@eee.hku.hk).

Peng Li is with the Department of Electrical & Electronic Engineering, Imperial College London (e-mail: peng.li13@imperial.ac.uk).

T. Parisini is with the Department of Electrical & Electronic Engineering, Imperial College London (e-mail: t.parisini@imperial.ac.uk).

S.Y.R. Hui is with Department of Electrical & Electronic Engineering, The University of Hong Kong (e-mail: ronhui@eee.hku.hk) and also with Imperial College London (e-mail: r.hui@imperial.ac.uk).

a variant of traditional approach for computational savings. Such technique is also referred to as the modified harmonic domain [18]. From the practical perspective, some issues can be caused by improper application of DFT (e.g., asynchronous sampling) [26], including an aliasing effect, spectral leakage, and picket-fence effect. In [13], the leakage effect is addressed by adaptively adjusting the window width for DFT. An alternative solution is proposed in [16] aiming at restoring the spectral leakage energy. It is shown that the inherent errors due to the leakage effects consisting in measurement devices can be fixed by this recursive group harmonic power minimizing strategy. On the other hand, the picket-fence effect is dealt with in [27] by a FT-based approach with interpolatory polynomial approximation for waveform reconstruction. Very recently, a multiple-interharmonics spectrum separation algorithm is proposed to distinguish intensive interharmonics in the case the signal is asynchronously sampled [33]. Apart from the DFT, the ESPRIT and Prony-based methods represent valid alternatives within the frequency domain but offers high-frequency-resolution DFT at the price of more computational requirements [14]. The subspace-least mean square method is recently proposed in [30] for highly accurate estimation of interharmonics under a noisy environment with a data sampling window of 1/30s only. Due to the complexity, high-resolution methods are suitable only for off-line analysis and benchmark. Another significant category of interharmonic detection methods involves the adaptive signal processing techniques based on a filter bank with adaptive parameter estimation in the time domain rather than the frequency domain [29]. More specifically, by linking n phase-locked loop (PLL) units within one “external" loop, the architecture devised in [20] succeeds in extracting the harmonics and inter-harmonics from a multi-sinusoidal measurement. The multi-PLL scheme is then enhanced by incorporating down-sampler for each PLL unit to reduce the computational effort of the overall estimator [28]. By replacing the PLLs with a bank of adaptive notch-filters (ANF), a new scheme is developed in [21] showing advantageous from a computational perspective in comparison with the PLL counterpart reported in [20]. Noticeably, because of the unknown initial conditions, the adaptive approaches (i.e., PLL and ANF) have slower dynamic response compared to DFT despite the merit in terms robustness and ease frequency additivity. Detailed comparison of commonly used interharmonic detection techniques are performed in [32]. In practice, the Field Programmable Gate Array (FPGA) architectures offers a very cost effective solution for implementing complicated algorithm for harmonic and interharmonics monitoring [31].

With the aim of improving the convergence speed of a time-domain method without significantly increasing the computation burden. A novel kind of kernel-based algorithms has been recently proposed for estimating n sinusoidal components with arbitrary frequencies [22]. This class of algorithms has been adopted for fast detection of fundamental and harmonics for grid-connected power electronics equipment [23]. The basic theory is based on a rather complex mathematical framework which is beyond the scope of this paper. While the original algorithm can estimate multiple frequency components including the fundamental, harmonics and interharmonics, the objective of this paper is to adopt this theory in a specific form to explore the use of this estimator for fast and accurate tracking of the fundamental and a single interharmonic within specified frequency band in the ac mains. Practical results are included to verify the feasibility and fast response of the proposed method.

## II. PROBLEM STATEMENT AND PRELIMINARIES

In this section, the generic algorithm for fast detection of signals of *n* (arbitrary) frequencies is introduced. Equations (1) to (20) are used to explain the general concept of multiple frequency detection in Section II to Section III. Then, the estimator will be adopted for the specific application and implementation of tracking the fundamental and an interharmonic (which is far from the fundamental frequency and is not an integral multiple of the fundamental frequency) in Section IV. This estimator is therefore specially designed for detecting the emerging problem of oscillations between parallel-connected PV inverters with LCL filters.

Consider a power electrical signal comprising a fundamental signal ($y_1(t)$) of nominal frequency $\omega_1$, plus other high-frequency components and a DC offset ($A_0$).

$$y(t) = A_0$$

$$= A_0 + A_1 \sin(\omega_1 + \emptyset_1) + \sum_{k=2}^{n} A_k \sin(\omega_k + \emptyset_k) \quad (1)$$

where $A_k, \omega_k$ and $\phi_k$ are the amplitude, frequency and initial phase of $y_k(t)$, respectively. The amplitudes verify the inequality $A_k \geq 0, k = 0, 1, \cdots$, the frequencies parameters are strict-positive and unique: $\omega_k > 0, \omega_k \neq \omega_j$ for $k \neq j$ and $\phi_k$ is the unknown initial phase of each sinusoid. Note that the fundamental component is isolated in (1) due to its importance in the context of power system signals. Note that the *k*-th component $y_k$ usually represents the *k*-th order harmonic, characterized by harmonic frequency.

$$\omega_k = k\omega_1 \quad (2)$$

In case only harmonics are present, the frequencies of the harmonic components need not to be independently estimated and can be derived from (2) by using the estimate of the fundamental frequency. However, the presence of inter-harmonics is inevitable in practical applications (i.e., $\omega_k$ may vary within a neighborhood of $k\omega_1$), thus motivating us to propose this algorithm that can estimate frequencies of all components independently. In view of (1), each sinusoidal component $y_k$ verifies the second order differential equation $\ddot{y}_k(t) = -\omega_k^2 y_k(t)$.

In the Laplace domain,

$$s^2 y_k(s) - s y_k(0) - \dot{y}_k(0) = -\omega_k^2 y_k(s) \quad (3)$$

where *s* is Laplace variable. By rearranging (3),

$$y_k(s) = \frac{s y_k(0) + \dot{y}_k(0)}{s^2 + \omega_k^2}$$

Hence, the signal $y(t)$ in the s-domain is expressed as

$$y(s) = \sum_{k=1}^{n} \frac{s y_k(0) + \dot{y}_k(0)}{s^2 + \omega_k^2} + \frac{A_0}{s}$$

which has a characteristic polynomial denoted by $P(s)$ with purely imaginary roots occurring in the a complex-conjugate pair at each frequency:

$$P(s) = s \prod_{k=1}^{n} (s^2 + \omega_k^2) = s^{2n+1} + a_{n-1} s^{2n-1} + \cdots + a_1 s^3 + a_0 s \quad (4)$$

It is worth noting that the frequencies $\omega_k$ act as the zeros of $P(s)$. Based on (4), the incoming signal $y(t)$ defined in (1) can be thought as generated by the following autonomous system the eigenvalue of which is identical to the zeros of the characteristic polynomial $P(s)$ [34]:

$$\begin{cases} \dot{x}(t) = A_x x(t) \\ y(t) = c_x^T x(t) + A_0 \end{cases} \quad (5)$$

where

$$\mathbf{A}_x = \begin{bmatrix} 0 & 1 & 0 & \cdots & 0 \\ -a_{n-1} & 0 & 1 & \cdots & 0 \\ \vdots & \ddots & \ddots & \ddots & \vdots \\ 0 & 0 & \ddots & \ddots & 1 \\ -a_0 & 0 & \cdots & \cdots & 0 \end{bmatrix}, \quad c_x^T = [1 \quad 0 \cdots 0 \quad 0]$$

In the following discussion, an algorithm that can estimate system's parameters $a_i, i = 0, 1, 2, \cdots$ in a very fast manner is proposed. The frequencies $\omega_k$ can be determined from $a_i$ through the relationship implied in (4) (i.e., the roots of the equation $P(j\omega) = 0$).

Comparing to the available methods that mainly deal with the fundamental and harmonic frequencies, the proposed multi-frequency strategy offers the flexibility of being able to address more than one sinusoid. This important feature offers a solution to fast online interharmonic detection. As clearly shown in (5), the order of the signal generator model depends on the number of frequencies to be estimated. The residual sinusoidal components (that are not taken into account) are implicitly treated as a disturbance which may result in a degradation of accuracy. However, higher computing load is required by increased dynamic order. In this connection, the computation burden and the precision need to be compromised. Without loss of generality, a generic framework that copes with *n* harmonics and a possible offset (see (1)) is dealt with in the next section.

## III. FREQUENCY TRACKING METHOD BASED ON INTEGRAL OPERATORS

### A. Preliminaries

In this section, an estimation scheme is designed for estimating *n* arbitrary frequencies in a harmonic signal. The fundamental theory behind this method is based on rather complex mathematics, but the suitably designed algorithm can be simply implemented via linear state-space equations. Next, we introduce some basic theory that contribute the further analysis, while the detailed derivation are reported in Appendix.

In this paper, we resort to a typical linear integral operator (see [22], [35] for more details), defined as

$$[V_K u](t) \triangleq \int_0^t K(t,\tau) u(\tau) d\tau, \quad t \in \mathbb{R}_{\geq 0} \quad (6)$$

where $u(t)$ is the processed signal and the function $K(t,\tau)$ is a specialized bivariate kernel function with the form:

$$K(t,\tau) \triangleq e^{-\rho(t-\tau)} (1 - e^{-\rho\tau})^{2n+1} \left[1 - e^{-\rho(t-\tau)}\right]^{2n+1} \quad (7)$$

where $\rho > 0$ is a design parameter. In the rest of the paper, we denote the *i*-th order signal derivative as $u^{(i)}, i = 0,1,2, \cdots$ for the sake of simplifying the notation. Moreover, given that a kernel function $K(t,\tau)$ has two variables, the *i*-th order derivative of *K* with respect to the second argument will be denoted as $K^{(i)}$. The reason for selecting the kernel function is that the integral operator of the derivative $u^{(i)}(t)$ through the specialized kernel $K(t,\tau)$ can be computed by using the image of the available signal $u(t)$ (proof is provided in Appendix A), that is

$$\left[V_K u^{(i)}\right](t) = (-1)^i \left[V_{K^{(i)}} u\right](t)$$

It is worth noting that the *i*-th derivative of the kernel (7) with respect to the second argument can be expressed as:

$$K^{(i)}(t,\tau) = \sum_{j=1}^{2n+2} e^{-\rho j t} f_{i,j}(\tau) \quad (8)$$

where $f_{i,j}(\cdot)$ are univariate functions of $\tau$. Let $K_{i,j}(t,\tau) \triangleq (-1)^i e^{-\rho j t} f_{i,j}(\tau)$; then by linearity of the integral operator, it follows that

$$\left[V_K u^{(i)}\right](t) = (-1)^i \left[V_{K^{(i)}} u\right](t) = \sum_{j=1}^{N+1} \left[V_{K_{i,j}} u\right](t)$$

Next, we apply the aforementioned results to devise the fast estimation scheme.

### B. Frequency Tracking Strategy

Now let us introduce the differential constraint model of (5):

$$y^{(2n)}(t) = \sum_{i=0}^{n-1} a_k y^{(2i)}(t) - a_0 A_0 \quad (9)$$

By taking the 1-st order time-derivative on both sides of the structural constraint (9), we obtain:

$$y^{(2n+1)}(t) = \sum_{i=0}^{n-1} a_i y^{(2i+1)}(t) \quad (10)$$

Then we apply the integral operator (6) on both sides of (10), getting to

$$\left[V_{K_{2n+1}} y^{(2n+1)}\right](t) = \sum_{i=0}^{n-1} a_i \left[V_{K_{2n+1}} y^{(2i+1)}\right](t) \quad (11)$$

For the sake of brevity, let $r_i(t) = \left[V_{K_{2n+1}} y^{(i)}\right](t), i = 0,1,\cdots 2n+1$, (11) can be rewritten as

$$r_{2n+1}(t) = \sum_{i=0}^{n-1} a_i r_{2i+1}(t) \tag{12}$$

By introducing the true parameter vector

$$\theta^* \triangleq [a_0 \quad a_1 \cdots \ a_{n-2} \quad a_{n-1}]^T,$$

and the vector of auxiliary signals that collect only the odd derivative indices

$$z(t) \triangleq [r_1(t), \quad r_3(t) \quad \cdots \quad r_{2n-1}(t)]^T$$

Equation (12) can be rewritten in a compact form as

$$z^T(t)\theta^* = r_{2n+1}(t) \tag{13}$$

The modulated signal $r_i(t), i = 0,1,\cdots,2n+1$ can be obtained as the output of an $(2n+2)$ -th dimensional linear time-varying dynamical system, described as (the derivation is given in Appendix B):

$$\begin{cases} \xi_i^{(1)}(t) = \boldsymbol{G}\xi_i(t) + \boldsymbol{E}_i(t)y(t) \\ r_i(t) = \boldsymbol{H}\xi_i(t) \end{cases} \tag{14}$$

with $\xi_i(0) = 0$ and where the other quantities in (14) are

$$\mathbf{G} = \mathrm{diag}(-\rho, -2\rho, \cdots, -\rho(2n+2))$$

$$\mathbf{E}_i(t) = \begin{bmatrix} K_{i,1}(t,t) \\ \vdots \\ K_{i,2n+2}(t,t) \end{bmatrix} \tag{15}$$

$$H = [1,1.\cdots,1]$$

By employing $n+1$ systems of the kind (14) comprising the set of $\mathbf{E}_i(t), \forall 1,3,\cdots,2n+1$ , both the vector of signals $z(t)$ and $r_{2n+1}$ (that are needed to form the constraint (13)) can be determined.

Note that (13) represents a standard linear expression for identification. Conventional augmentation tools used in system identification can be employed to form a well-posed algebraic system based on (13). Let us first multiply both sides of (13) by $z(t)$:

$$R(t)\theta^* = S(t) \tag{16}$$

where $R(t)$ and $S(t)$ are the so-called auto-covariance and cross-covariance matrices defined as

$$R(t) \triangleq z(t)z^T(t), \quad S(t) \triangleq z(t)r_{2n+1}(t),$$

In order to avoid singularity of the instantaneous auto-covariance matrix R(t) (i.e., rank 1 at any time instant). We apply to both sides of (16) a simple second order low-pass filter that is described by transfer function representation:

$$F(s) = \frac{w_c^2}{s^2 + \lambda w_c s + w_c^2} \tag{17}$$

for faster frequency response than the first order, while maintaining a low level of complexity.

Therefore, the following relationship holds for all $t \geq 0$

$$\mathcal{L}^{-1}\{F(s)R(s)\}(t)\theta^* = \mathcal{L}^{-1}\{F(s)S(s)\}(t) \tag{18}$$

where $\mathcal{L}^{-1}$ denotes the operation of the inverse Laplace transform. Defining $\mathrm{R_f(t)} = \mathcal{L}^{-1}\{\mathrm{F(s)R(s)}\}\mathrm{(t)}$ and $\mathrm{S_f(t)} = \mathcal{L}^{-1}\{\mathrm{F(s)S(s)}\}\mathrm{(t)}$, an estimate $\hat{\theta}(t)$ of the parameter vector $\theta^*$ can be obtained by minimizing the quadratic criterion

$$\hat{\theta}(t) = \arg\min_{\theta^*} ||R_f(t)\theta^* - S_f(t)|| .$$

In this case, the unknown parameter vector $\theta^*$ can be estimated by

$$\hat{\theta}(t) = \begin{cases} \theta_0 & t < t_\epsilon \\ R_f(t)^{-1}S_f(t), & t \geq t_\epsilon \end{cases} \tag{19}$$

where $\theta_0$ is a guessed parameter vector depending on the nominal frequency values, and $t_\epsilon > 0$ is a small time constant, needed because $\mathrm{R_f(t)}$ is not invertible at t = 0 (i.e., $\mathrm{R_f}$ (0) = 0). Finally, as mentioned before, the frequencies $\omega_1, \ldots, \omega_n$ are computed by letting

$$P(j\omega) = 0 \tag{20}$$

where $P(j\omega)$ is parametrized by $a_i$ as given in (4).

A structural block diagram of the proposed algorithm is shown in Fig. 1, where the $n+1$ identical system (see (14)) are enhanced by dotted rectangles and $y(t)$ is the incoming signal.

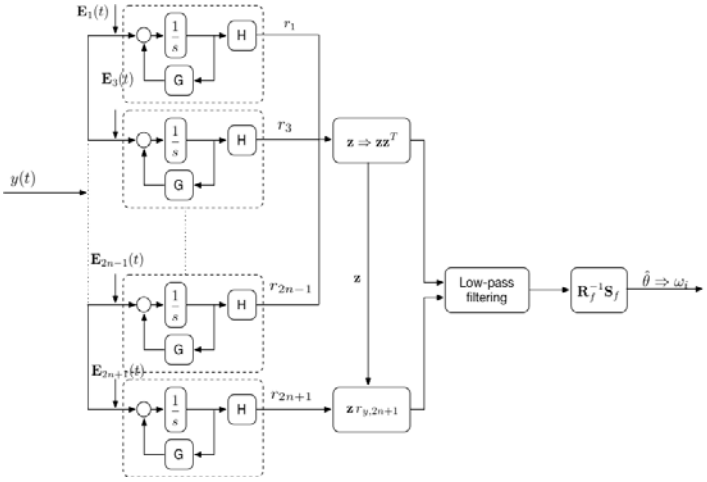


Fig.1 Block diagram of the proposed algorithm

**Remark 1:** Note that the algebra algorithm (19) is valid only when the filtered auto-covariance matrix $R_f(t)$ is invertible. The invertibility of $R_f(t)$ characterizes a sufficiently informative output signal at time $t$. In view of (14), the parameter $\rho$ determines the poles of **G** that in turn determines the cut-off frequency of the overall low-pass filtering structure. A larger $\rho$ results in a poorer noise immunity, while a smaller $\rho$ may result in a less informative $R_f(t)$ due to the excessive attenuation of $y(t)$. To this end, the choice of $\rho$ depends on a priori information of the frequency band of the interharmonic.

**Remark 2:** The low-pass filter (17) is applied on both sides of (18), then the parameter vector $\hat{\theta}(t)$is determined algebraically by $R_f(t)^{-1}S_f(t)$ by which the estimation results are independent of the low pass filter. However, to avoid excessive attenuation that may lead to numerical issue, the rules given in Remark 1 also apply to the design of filtering parameter $\lambda$ and $w_c$.

## IV. Adoption Of The Algorithm For Tracking Fundamental And Interharmonic Components

In this section, the proposed estimator is adopted for detecting and tracking the fundamental and a typical interharmonics. For practical applications of grid-connected power inverters, the fundamental frequency is selected as 50 Hz and the interharmonic frequency as 1.94kHz (representing the occurrence of resonance between parallel grid-connected power inverters). Note that the use of the integral observer algorithm for detecting total harmonics has been reported in [23] and is thus not repeated here. The mains voltage signal can be expressed as:

$$v(t) = v_1(t) + v_m(t) + \sum_{k=2}^{n\backslash m} v_k\,(t) \tag{21}$$

where $t$ is the time variable, $v_1(t)$ is the fundamental voltage, $v_m(t)$ is the inter-harmonic that needs to be identified and $\sum_{k=2}^{n\backslash m} v_k\,(t)$ is the total harmonic voltage apart from $v_m(t)$. For the sake of further analysis, let us consider

$$y(t) = v_1(t) + v_m(t)$$

It is important to note that the estimator considers the remaining harmonics $\sum_{k=2}^{n\backslash m} v_k\,(t)$ as 'noise' initially. The schematic of this method is shown in Fig. 2. It should be noted that the band-stop filter is employed to attenuate the impact of the 'noise' term (harmonics and pure noise) since the magnitude of the inter-harmonic is very small. The band-stop filter is an elliptic type with 80Hz and 1800Hz respectively for the lower and upper passband edge. Although the elliptic filter suffers from passband and stopband ripples, it is chosen for its fast frequency response which is an important attribute for this application.

Now, $y(t)$ can be thought as generated by the following autonomous system

$$\begin{cases} \dot{x}(t) = A_x x(t) \\ y(t) = c_x^T x(t) \end{cases} \tag{22}$$

where

$$\mathbf{A}_x = \begin{bmatrix} 0 & 1 & 0 & 0 \\ a_1 & 0 & 1 & 0 \\ 0 & 0 & 0 & 1 \\ a_0 & 0 & 0 & 0 \end{bmatrix},$$

$$c_x^T = [1 \quad 0 \quad 0 \quad 0]$$

The state-space system (22) leads to the next differential constraint model:

$$y^{(4)}(t) = a_1 y^{(2)}(t) + a_0 y(t) \tag{23}$$

Applying the linear integral operator to both side of (23) with a kernel function in the form of (6) with the order of the multiplier reduced from 2$n$+1 to 4 and $\rho$ is designed as 1000

$$K(t,\tau) \triangleq e^{-1000(t-\tau)}(1-e^{-1000\tau})^4\left[1-e^{-1000(t-\tau)}\right]^4$$

we obtain

$$r_4(t) = [r_0(t) \quad r_2(t)]\begin{bmatrix} a_0 \\ a_1 \end{bmatrix} = z^T(t)\theta^* \tag{24}$$

where $r_i(t) = \left[V_K y^{(i)}\right](t), i = 0, 2, 4.$

Moreover, $r_i(t), i = 0, 2, 4$ can be respectively obtained as the output of a 5-th order linear time-varying dynamical system, described as:

$$\begin{cases} \xi_i^{(1)}(t) = \boldsymbol{G}\xi_i(t) + \boldsymbol{E}_i(t)y(t) \\ r_i(t) = \boldsymbol{H}\xi_i(t) \end{cases}$$

with $\xi_i(0) = 0$ and

$$\mathbf{G} = \text{diag}(-1000, -2000, -3000, -4000, -5000)$$

$$\mathbf{E}_i(t) = \begin{bmatrix} K_{i,1}(t,t) \\ K_{i,2}(t,t) \\ K_{i,3}(t,t) \\ K_{i,4}(t,t) \\ K_{i,5}(t,t) \end{bmatrix}, \tag{25}$$

$$H = [1 \quad 1 \quad 1 \quad 1 \quad 1].$$

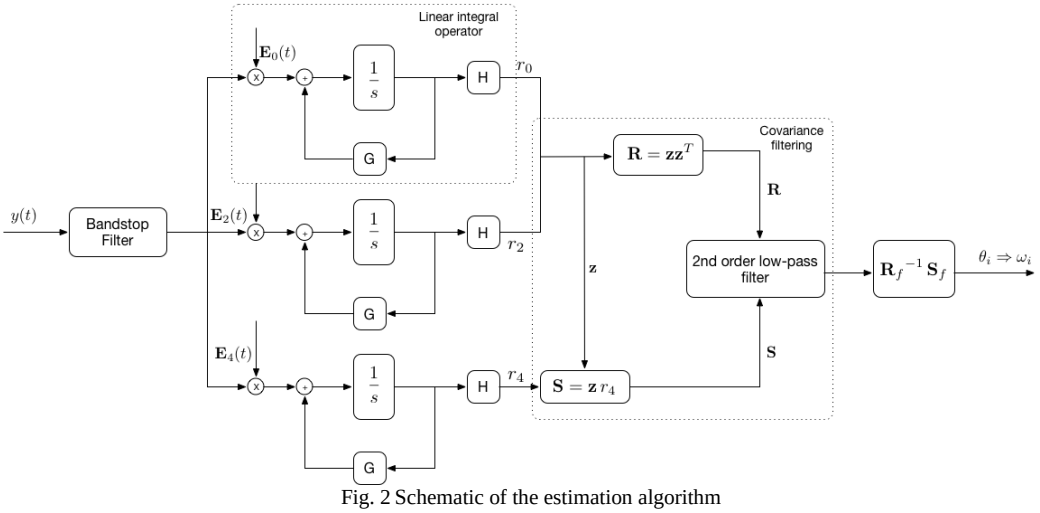


Fig. 2 Schematic of the estimation algorithm

Note that the elements of $\mathbf{E}_i(t),\ i = 0, 2, 4$ can be determined based on (8) by symbolic computation tools. The expressions are given as follows:

$$\mathbf{E}_0(t) = \begin{bmatrix} K_{0,1}(t,t) \\ K_{0,2}(t,t) \\ K_{0,3}(t,t) \\ K_{0,4}(t,t) \\ K_{0,5}(t,t) \end{bmatrix} = \begin{bmatrix} -1000(3e^{-1000t}+1)(e^{-1000t}-1)^3 \\ 8000(e^{-1000t}+1)(e^{-1000t}-1)^3 \\ -6000(e^{-1000t}+3)(e^{-1000t}-1)^3 \\ 16000(e^{-1000t}-1)^3 \\ 1000(e^{-1000t}-5)(e^{-1000t}-1)^3 \end{bmatrix}$$

$$\mathbf{E}_2(t) = \begin{bmatrix} K_{2,1}(t,t) \\ K_{2,2}(t,t) \\ K_{2,3}(t,t) \\ K_{2,4}(t,t) \\ K_{2,5}(t,t) \end{bmatrix}$$

$$= \begin{bmatrix} -1000^3(27e^{-4000t} - 32e^{-3000t} + 6e^{-2000t} - 1) \\ 16 * 1000^3(2e^{-4000t} - e^{-3000t} + e^{-1000t} - 2) \\ -6 * 1000^3(e^{-4000t} - 6e^{-2000t} + 32e^{-1000t} - 27) \\ 16 * 1000^3(e^{-3000t} - 12e^{-2000t} + 27e^{-1000t} - 16) \\ 1000^3(e^{-4000t} - 32e^{-3000t} + 162e^{-2000t} - 256e^{-1000t} + 125) \end{bmatrix}$$

$$\mathbf{E}_4(t) = \begin{bmatrix} K_{4,1}(t,t) \\ K_{4,2}(t,t) \\ K_{4,3}(t,t) \\ K_{4,4}(t,t) \\ K_{4,5}(t,t) \end{bmatrix}$$

$$= \begin{bmatrix} -1000^5(243e^{-4000t} - 128e^{-3000t} + 6e^{-2000t} - 1) \\ 16 * 1000^5(8e^{-4000t} - e^{-3000t} + e^{-1000t} - 8) \\ -6 * 1000^5(e^{-4000t} - 6e^{-2000t} + 128e^{-1000t} - 243) \\ 16 * 1000^5(e^{-3000t} - 48e^{-2000t} + 243e^{-1000t} - 256) \\ 1000^5(e^{-4000t} - 128e^{-3000t} + 1458e^{-2000t} - 4096e^{-1000t} + 3125) \end{bmatrix}$$

Finally, (24) can be solved by following the same steps shown in the generic case:

**Step 1:** Multiplying both sides of (24) by $z(t)$ leads to:

$$R(t)\theta^* = S(t) \tag{26}$$

with

$$R(t) \triangleq z(t)z^T(t), \quad S(t) \triangleq z(t)r_4(t).$$

**Step 2:** Apply to both sides of (26) a low-pass filter in the form of (17), with $\lambda = 4, w_c = 350$.

$$F(s) = \frac{w_c^2}{s^2 + \lambda w_c s + w_c^2}$$

such that

$$\mathrm{R_f(t)}\theta^* = \mathrm{S_f(t)}(t) \tag{27}$$

where $\mathrm{R_f(t)} = \mathcal{L}^{-1}\{\mathrm{F(s)R(s)}\}(\mathrm{t})$ and $\mathrm{S_f(t)} = \mathcal{L}^{-1}\{\mathrm{F(s)S(s)}\}(\mathrm{t})$.

**Step 3:** The estimate $\hat{\theta}(\mathrm{t}) = [a_0 \quad a_1]^T$ of the unknown parameter vector $\theta^*$ is obtained by

$$\hat{\theta}(t) = \begin{cases} \theta_0 & t < t_\epsilon \\ R_f(t)^{-1}S_f(t), & t \geq t_\epsilon \end{cases} \tag{28}$$

where $\theta_0$ is a guessed parameter vector depending on the nominal frequency values, and $t_\epsilon > 0$ is a small time constant. $t_\epsilon > 0$ is needed because $R_f(t)$ is not invertible at $t = 0$ (i.e., $R_f\ (0) = 0$).

**Step 4:** The frequencies $\omega_1$ and $\omega_m$ of the fundamental and the inter-harmonic are indirectly estimated as the roots of the following equation

$$s^4 - a_1 s^2 - a_0 = 0 \tag{29}$$

The coefficients of $a_0$ and $a_1$ have to be dynamically determined through Step 1 to Step 3. If only the fundamental component exists, (29) provides only one unique real solution. If both of the fundamental and interharmonics are present, it gives two unique solutions.

For fast detection of the interharmonic, the matrix $R_f(t)$ is utilized in addition to the frequency estimates. Let us consider $\sigma_{min}(R_f(t))$ as the minimum eigenvalue of $R_f(t)$. According to the concept of persistency of excitation, $\sigma_{min}(R_f(t))$ can be used as an indicator to capture the existence of the interharmonic [25]. More specifically, when the algorithm is fed by a combination of fundamental and interharmonic, $\sigma_{min}(R_f(t))$ is inherently sinusoidal with the mean above a certain level depending on the amplitude of the input in the steady state. As soon as the interharmonic vanishes, $\sigma_{min}(R_f(t))$ quickly decays and moves back only when the interharmonic appears again. In this connection, we proposed a mechanism for estimating interharmonic with a properly designed threshold. The frequency estimate of the interharmonic is driven to 0 (an indication of no interharmonic) as soon as $\sigma_{min}(R_f(t))$ falls below the threshold. On the other hand, the initial condition of the frequency estimates is reset by a value within the possible range of interharmonic frequency when the indicator reach the threshold again, thus significantly saving the time for convergence.

## V. Experimental Verification

In order to evaluate the effectiveness of the proposal method in detecting the fundamental and interharmonic, a programmable power supply is used to generate the required voltage waveforms. Because the proposed algorithm provides numerical values of the frequency components, digital-to-analogue (D/A) converters are used to generate analogue signals that represent the fundamental and interharmonics components. The fundamental frequency is 50 Hz, while the targeted interharmonic is within the targeted frequency band of 1.7 kHz to 2.0 kHz (using the examples of [11] and [12]). The algorithm is implemented in a dSpace DS1006 system with a CPU clock rate of 2.8GHz and a memory size of 1GB (SDRAM) (Fig.3). The sampling frequency of the dSpace system is 10 kHz. Because of the widely separated fundamental frequency and the interharmonic, their frequency values are scaled with the frequency-to-voltage ratios of 1:10 and 1:25, respectively, so that the frequency values can be displayed as voltage signals in a digital storage oscilloscope in real time. In this section, the fundamental frequency, the interharmonic frequency and the input signal are in the measured waveforms in the figures as the green, blue and yellow traces respectively.

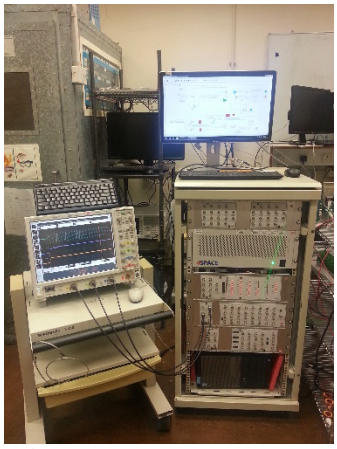

Fig.3 A photograph of the experimental setup with the dSpace system and digital oscilloscope.

### *A Steady State Estimation*

The first test is to generate a fundamental signal at 50 Hz with a superimposed high frequency signal at 1.94 kHz (i.e. representing the interharmonic). This signal is sampled by the dSpace A/D system, and digitized for use in the proposed algorithm. The sampling rate of the dSpace system is 10 kHz, meaning that the adopted algorithm can be executed within 100$\mu$s. The computational time of the algorithm in the dSpace system is about 55$\mu$s. The actual and computed fundamental frequency and interharmonic frequency are displayed in Fig.4 and tabulated in Table 1. These results show that the practical and computed frequencies are in good agreement. Adding extra frequency detection functions will inevitably increase the computational burden of the microcontroller of the power inverter. If such computational needs exceed the computational capabilities (e.g. speed) of the microcontroller, additional processor may be needed to implement the frequency detection functions.

TABLE 1

| | Fundamental frequency | Interharmonic frequency |
|---|---|---|
| Actually programmed in power source | 50.000 | 1.94 kHz |
| Computed by proposed method | 50.007 | 1.99 kHz |

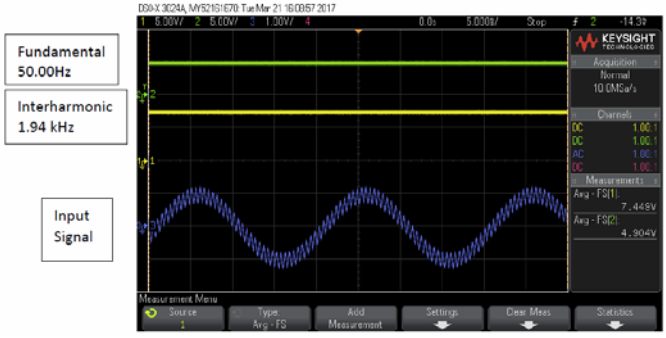


Fig. 4 Practical input signal with fundamental frequency of 50Hz superimposed with an interharmonic of 1.94kHz, and the analog versions of the computed fundamental and interharmonic frequency (5ms/Div.)

### *B Sudden Appearance of Interharmonic*

The second test emulates the sudden occurrence of the resonance of the LCL filters between parallel PV systems. The power source is programmed initially with the fundamental component of 50Hz only. Then the interharmonic component is added to the fundamental component. The measured input voltage signal provided by the power source is shown with the analogue version of the fundamental frequency and interharmonic frequency in Fig.5. The time scale is set at 5 ms/div. It can be observed that the fundamental frequency remains constant through the test, because its analogue version remains a straight horizontal line during the step change of the interharmonic.

The kernel signal is used to provide fast detection of the interharmonic. It is the eigenvalue of the matrix signal $R_f(t)$ which is composed of processed versions (filtered) of the incoming signal $y(t)$. So the kernel signal is an inherent sinewave because of the sinusoidal nature of $y(t)$. When the inharmonic is absent, the kernel signal is zero. When the interharmonic appears, the kernel signal increases from zero. Therefore, when the kernel signal increases beyond a threshold $\Delta V_1$, it can trigger the signal of interharmonic occurrence from 0 to 1. The kernel signal will then rise until it settles down to a steady-state level (with a sinusoidal ac ripple). A moving window method is used to locate the minimum kernel value for each period of the kernel signal (i.e. half period of the mains voltage). When the interharmonic disappears, the kernel signal will decay to zero. Thus, when the kernel signal is less than the minimum kernel value by another threshold $\Delta V_2$, it can trigger the signal of the interharmonic occurrence from 1 to 0. As long as the thresholds $\Delta V_1$ and $\Delta V_2$ are slightly larger than the noise level, the detection times can be minimized. In the practical tests, $\Delta V_1$ and $\Delta V_2$ are set at 0.098V and 0.188V, respectively.

It is however important to note that the harmonic detection time from 0 to 1 is usually very fast because the initial kernel signal is zero and has no ripple. This feature is important and advantageous because the purpose of the algorithm is to detect the occurrence of the interharmonic in this specific application as the signal for the occurrence of resonance between parallel grid-connected power inverters. In Fig.5, the detection time for the occurrence of the interharmonic is only 3ms. This detection time can be reduced if $\Delta V_1$ is further reduced, as long as $\Delta V_1$ is larger than the noise level in the practical implementation.

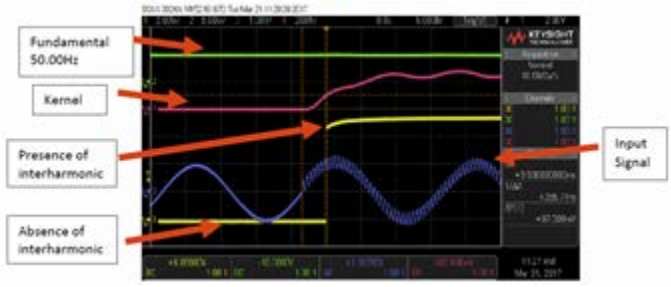


Fig. 5 Practical input signal with fundamental frequency of 50Hz superimposed with an interharmonic of 1.94kHz, and the analog versions of the computed fundamental and interharmonic frequency (5ms/Div.)

### *C Sudden Disappearance of Interharmonic*

The third test focuses on the sudden disappearance of the interharmonic. This is to emulate the situation that the resonance between the parallel LCL filters has stopped. The

corresponding measured signals are displayed in Fig.6. Fig.5 shows that the kernel signal will reach its steady waveform within about one mains cycle. Such waveform is used again for detecting the disappearance of the interharmonic. When the kernel value falls to a value less than the minimum value by a certain threshold, it signifies the absence of the interharmonic. In this case, it takes about 9ms to detect the disappearance of the interharmonic. This detection time is less than half of a mains cycle. In Fig.6, the kernel signal at the high state has some ripple. The trigger signal has to wait for the kernel signal to drop below the minimum kernel signal in the moving window by $\Delta V_2$ before changing from 1 to zero. This is why the detection time for the disappearance of the interharmonic is longer than that for the occurrence of the interharmonic.


Fig. 6 Practical input signal with fundamental frequency of 50Hz superimposed with an interharmonic of 1.94kHz, and the analog versions of the computed fundamental and interharmonic frequency (5ms/Div.)

*D Variation of Mains Frequency*

The fourth test considers the possibility of mains frequency variation due to the increasing use of intermittent renewable energy penetration in power grid, especially microgrid using small electric generators. Normally, large-scale power grids do not have rate of change of frequency (RoCoF) higher than 0.1 Hz per second. For U.K., the RoCoF is limited at 0.2 Hz/s [24]. For microgrid, a higher RoCoF of 0.5 Hz/second is adopted in this test. The RoCoF is programmed in a linear manner so that the frequency value ramps up and down between 48 Hz and 52 Hz. For a RoCoF of 0.5 Hz/s, the mains frequency changes from 48 Hz to 52 Hz in 8 seconds.

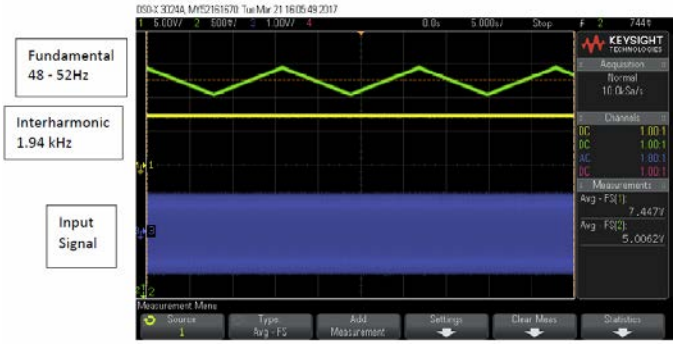


Fig.7 Practical input signal with fundamental frequency (48-52Hz) superimposed with an interharmonic of 1.94kHz, and the analog versions of the computed fundamental and interharmonic frequency (5 s/Div.)

Fig.7 shows the input signal comprising the fundamental frequency superimposed with an interharmonic of 1.94 kHz, with the fundamental frequency varying between 48 Hz and 52 Hz. It can be seen that the analog version of the fundamental frequency varies within 48 Hz and 52 Hz linearly as expected, while the analog version of the interharmonic frequency remains constant. These results indicate that, even if the mains frequency varies, the successful detection of interharmonic remains intact.

*E Further Discussion*

For the targeted interharmonic frequency range of 1.7 kHz to 2 kHz, the choice of 1.94 kHz in previous section represents the upper end of the range. The proposed method has been tested with an interharmonic of 1.64 kHz, which is at the lower end of the range. The fundamental frequency remains at 50 Hz. Fig.8 shows the measurements when a smaller threshold ($\Delta V_1$) is is adopted. Note that the time scale of Fig.8 is 2ms/div. (instead of 5ms/div. as in Figs. 3-5). With a lower threshold, the detection time is reduced to about 1.5ms. Therefore, for the typical interharmonic frequency range of 1.7 kHz to 2 kHz reported in [11][12], the proposed method can detect the occurrence of interharmonic within a few milliseconds. In principle, the proposed method can detect multiple frequencies. The demonstration in this paper is specific to potential applications such as resonance between parallel grid-connected power inverters.


Fig.8 Practical input signal with fundamental frequency of 50Hz superimposed with an interharmonic of 1.64kHz, and the analog versions of the computed fundamental and interharmonic frequency (2ms/Div.)

One possible application of the proposed algorithm is to detect the interharmonic arising from parallel operations of grid-connected inverters with LCL filters. Fig.9 shows a typical setup based on the LCL filter parameters previously reported in [8]. The inverters are operated at a switching frequency of 3.78 kHz. A real-time simulation on this setup is used to demonstrate the interharmonic oscillation between the power inverters. The total current injected into the grid is captured and outputted as a real-time signal for analysis with the proposed algorithm. Fig.10 shows the injected current waveform and the signals representing the fundamental component and interharmonic component (captured immediately when the test begins). The computed fundamental frequency is 49.66Hz and the interharmonic frequency is 1.387 kHz.

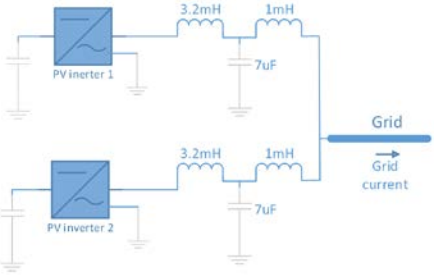


Fig.9 Schematic of a case study based on two parallel grid-connected inverters


Fig.10 Current injected into the grid and the signals of the fundamental and interharmonic components (5V/div. for the three traces; 50ms/div.)

The original algorithm [22] was designed to detect *n* unknown frequencies. Previously, it has been used to detect harmonics for active power filter applications. In this project, we demonstrate its use for the detection of the fundamental and interharmonics. Since the frequency estimates tend to converge to the frequencies with greater amplitude, the introduction of a band-pass filter is needed to identify the interharmonic (which typically has a much smaller amplitude than the fundamental frequency). But the cutoff frequency of the band-pass filter is hardly dependent on the interharmonic. In this application, it is simply set at a value higher than the fundamental frequency. If the information of the interharmonic is unknown, a higher-order estimation scheme of the general algorithm (that takes more frequencies into consideration) has to be adopted.

## VI. Conclusions

This paper presents the first practical implementation of an observer-based algorithm for fast detection of fundamental signal and interharmonic component. The theory behind the algorithm has been summarized and explained. The algorithm is adopted in a form for monitoring the presence of the mains frequency and the interharmonic and for estimating their values. A novel method of using the kernel signal for fast interharmonic detection has been proposed and practically demonstrated. Experimental results have confirmed that the detection times of the fundamental and interharmonic can be achieved within half of a mains cycle. This method is suitable for applications such as monitoring the occurrence of resonance between parallel LCL filters of grid-connected inverters.

## APPENDIX A

Assuming that the signal $u(t)$ admits the *i*-th order derivative for $t \geq 0$ and a kernel $K(t,\tau)$ that admits the *i*-th order derivative with respect to the second argument, the following relationship holds (obtained by means of the integration by parts [35]):

$$\begin{aligned}\left[V_K u^{(i)}\right](t) = &\sum_{j=0}^{i-1}(-1)^{i-j-1}u^{(j)}(t)K^{(i-j-1)}(t,t)\\ &+\sum_{j=0}^{i-1}(-1)^{i-j}u^{(j)}(0)K^{(i-j-1)}(t,0)\\ &+(-1)^i\left[V_{K^{(i)}}u\right](t)\end{aligned}$$

It implies that $\left[V_K u^{(i)}\right](\cdot)$ can be obtained by the lower-order time-derivatives of the processed signal $u, u^{(1)}, \cdots u^{(i-1)}$, which are usually unavailable in real-time. However, if a kernel $K$ verifies the following conditions:

$$K^{(j)}(t,0) = 0, \quad \text{(A1-a)}$$

$$K^{(j)}(t,t) = 0, \quad \text{(A1-b)}$$

for all $t \geq 0$ and , $i = 0,1,\cdots,i-1$, then the linear integral of a derivative signal $u^{(i)}$ can be expressed as

$$\left[V_K u^{(i)}\right](t) = (-1)^i\left[V_{K^{(i)}}u\right](t) \quad \text{(A2)}$$

where the right hand side only depends on the available kernel function $K$ and the signal $u(t)$ per se, thus evading the unavailability of signal derivatives.

By adopting the following bivariate function proposed in [35]

$$K(t,\tau) \triangleq e^{-\rho(t-\tau)}(1-e^{-\rho\tau})^N\left[1-e^{-\rho(t-\tau)}\right]^N \quad \text{(A3)}$$

the condition (A1-a) is met by the factor $(1-e^{-\rho\tau})^N$ up to $N$th order , while the condition (A2-b) is met by the third factor $(1-e^{-\rho(t-\tau)})^N$.

## APPENDIX B

We now describe how such a transformed signal can be obtained as the output of a linear system. First, Let $\xi(t) = [V_K u](t)$ (defined in (6)), by applying the Leibnitz rule in deriving the integral, the signal $[V_K u](t)$, for $t > 0$, can be obtained as the output of a dynamic system described as follows

$$\begin{cases}\xi^{(1)}(t) = \int_0^t \left(\frac{\partial}{\partial t}K(t,\tau)\right)u(\tau)d\tau + K(t,t)u(t)\\ [V_K u](t) = \xi(t)\end{cases} \quad (B1)$$

where $\xi(t) = \xi^{(1)}(t) = 0$.

Since the i-th derivative of the kernel (A3) with respect to the second argument can be expressed as:

$$K^{(i)}(t,\tau) = \sum_{j=1}^{N+1} e^{-\rho jt} f_{i,j}(\tau) \quad (B2)$$

where $f_{i,j}(\cdot)$ are univariate functions of $\tau$. Let $K_{i,j}(t,\tau) \triangleq (-1)^i e^{-\rho jt} f_{i,j}(\tau)$; then by linearity of the integral operator, it follows that

$$\left[V_K u^{(i)}\right](t) = (-1)^i\left[V_{K^{(i)}}u\right](t) = \sum_{j=1}^{N+1}\left[V_{K_{i,j}}u\right](t).$$

Moreover, letting $\xi_{i,j}(t) \triangleq \left[V_{K_{i,j}}u\right](t)$, with $i \in \{0,\cdots,n\}$, $j \in \{1,\cdots,N+1\}$, and taking into account that, for all $t \geq 0$, we have

$$K_{N|i,j}(t,0) = 0,$$

$$\frac{\partial}{\partial t}K_{N|i,j}(t,\tau) = -\rho j e^{-\rho jt} f_{N|i,j}(\tau).$$

Thanks to (B1), $\left[V_{K_N}u\right]$ admits the following $(N+1)$-th dimensional state-space realization:

$$\begin{cases}\xi_{i,j}^{(1)}(t) = -\rho j\xi_{i,j}(t) + K_{i,j}(t,t)u(t)\\ \left[V_K u^{(i)}\right](t) = \sum_{j=1}^{N+1}\xi_{i,j}(t)\end{cases} \quad (B3)$$

with $\xi_{i,j}(0) = 0, \forall j = 1,\cdots,N+1$.

## REFERENCES


[1] F. Blaabjerg, Z. Chen, and S. B. Kjaer, "Power electronics as efficient interface in dispersed power generation systems," IEEE Trans. Power Electron., vol. 19, no. 5, pp. 1184–1194, Sep. 2004.

[2] E. Twining and D. Holmes, "Grid current regulation of a three-phase voltage source inverter with an LCL input filter," IEEE Trans. Power Electron., vol. 18, no. 3, pp. 888–895, May 2003.

[3] J. H. R. Enslin and P. J. M. Heskes, "Harmonic interaction between a large number of distributed power inverters and the distribution network," IEEE Trans. Power Electron., vol. 19, no. 6, pp. 1586–1593, Nov. 2004.

[4] M. Liserre, R. Teodorescu, and F. Blaabjerg, "Stability of photovoltaic and wind turbine grid-connected inverters for a large set of grid impedance values," IEEE Trans. Power Electron., vol. 21, no. 1, pp. 263–272, Jan. 2006.

[5] R. Juntunen, J. Korhonen, T. Musikka, L. Smirnova, O. Pyrh¨onen, and P. Silventoinen, "Identification of resonances in parallel connected grid Inverters with LC- and LCL-filters", Proc. IEEE Appl. Power Electron. Conf. Expo., 2015, pp. 2122–2127.

[6] M. Lu, X. Wang, P.C. Loh, and F. Blaabjerg, "An analysis method for harmonic resonance and stability of multi-paralleled LCL-filtered inverters", Proc. IEEE 6th Int. Symp. Power Electron. Distrib. Gener. Syst., Aachen, Germany, 2015, pp. 1–6.

[7] M. Lu, X. Wang, P. C. Loh, and F. Blaabjerg, "Interaction and aggregated modeling of multiple paralleled inverters with LCL filter" , Proc. IEEE Energy Convers. Congr. Expo., 2015, pp. 1954–1959.

[8] M. Lu, X. Wang, P.C. Loh and F. Blaabjerb, "Resonance interaction of multiparallel grid-connected inverters with LCL filter", IEEE Trans. Power Electron., vol. 32, no. 2, Feb. 2017, pp: 894-899

[9] J.He, Y. Li, and D. Bosnjak, "Investigation and active damping of multiple resonances in a parallel-inverter-based microgrid," IEEE Trans. Power Electron., vol. 28, no. 1, pp. 234–246, Jan. 2013.

[10] X. Wang, F. Blaabjerg, M. Liserre, and Z. Chen, "An active damper for stabilizing power-electronics-based AC systems," IEEE Trans. Power Electron., vol. 29, no. 7, pp. 3318–3328, Jul. 2014.

[11] Xiaonan Lu ; Kai Sun ; Lipei Huang ; Marco Liserre ; Frede Blaabjerg, "An active damping method based on biquad digital filter for parallel grid-interfacing inverters with LCL filters", IEEE Applied Power Electronics Conference and Exposition (APEC), 2014 Twenty-Ninth Annual , 16-20 March 2014

[12] Haining Wang; Peng Zhang; Jianhui Su; Guorong Zhang, "Resonant mechanism of multi grid-connected inverters in distribution power systems", IEEE Energy Conversion Congress and Exposition (ECCE), 2015, Pages: 1729 - 1735

[13] T. X. Zhu, "Exact Harmonics/Interharmonics Calculation Using Adaptive Window Width", IEEE Transactions on Power Delivery, Year: 2007, Volume: 22, Issue: 4, Pages: 2279 – 2288

[14] I. Y.-H. Gu and M. H. J. Bollen, "Estimating interharmonics by using sliding-window ESPRIT," IEEE Trans. Power Del., vol. 23, no. 1, pp. 13–23, Jan. 2008.

[15] Mauricio Caixba; Abner Ramirez, "Enhanced switching function matrix calculation in the interharmonic domain", IEEE PES General Meeting, Year: 2010 Pages: 1 – 5

[16] H.C. Lin, "Power harmonics and interharmonics measurement using recursive group-harmonic power minimizing algorithm", IEEE Trans. Ind. Electron., vol.59, No.2, Feb. 2012, pp: 1184-1193

[17] P. Drabek and M. Pittermann, "Calculation of interharmonics of power electronic converters – using of harmonic analysis", Annals of Faculty Engineering Hunedoara International Journal of Engineering, 2011, pp: 151-154

[18] A. Ramirez, "The modified harmonic domain: Interharmonics", IEEE Trans. on Power Delivery, 2011, vol. 26, No. 1, pp: 235-241.

[19] H. C. Lin, "Fast tracking of time-varying power system frequency and harmonics using iterative-loop approaching algorithm," IEEE Trans. Ind. Electron., vol. 54, no. 2, pp. 974-983, Apr. 2007.

[20] Karimi-Ghartemani. M. and Iravani. M. R., "Measurement of harmonics/inter-harmonics of time-varying frequencies". IEEE Trans. on Power Delivery, 2005, vol. 20, No. 1, pp: 23–31.

[21] Mojiri, M., Karimi-Ghartemani, M. and Bakhshai. A., "Processing of harmonics and interharmonics using an adaptive notch filter". IEEE Trans. on Power Delivery, 2010, vol. 25, No. 2, pp:534–542.

[22] Boli Chen, Peng Li, Gilberto Pin and Thomas Parisini, "Estimation of Multi-Sinusoidal Signals: A Deadbeat Methodology", in Proc. of the IEEE Conf. on Decision and Control, Las Vegas, NV, USA, 2016.

[23] Chen B., Pin G., Ng. W.M., Parisini T. and Hui S.Y.R., "A Fast-Convergent Modulation Integral Observer for Online Detection of the Fundamental and Harmonics in Grid-Connected Power Electronics Systems", IEEE Transactions on Power Electronics, Vol.32, No.4, 2017, pp: 2596-2607

[24] M. Albu and R. Popovici, "Rate of change of frequency – a power quality descriptor", IEEE International Conference on Harmonics and Quality of Power (ICHQP), 25-28 May, 2014, pp: 312-316

[25] Chen B., Pin G., Ng. W.M., Chi K. Lee, Hui S.Y.R and Parisini T., "An Adaptive Observer-Based Switched Methodology for the Identification of a Perturbed Sinusoidal Signal: Theory and Experiments", IEEE Transactions on Signal Processing, Vol.62, No.24, 2014, pp: 6355-6365

[26] A. Testa, M. F. Akram, R. Burch et al., "Interharmonics: Theory and Modeling", IEEE Transactions on Power Delivery, Vol.22, No.4, 2007, pp: 2335-2348

[27] G.W. Chang, C.I. Chen, Y.J. Liu and M.C. Wu, "Measuring power system harmonics and interharmonics by an improved fast Fourier transform-based algorithm", IET Generation, Transmission & Distribution, Vol.2, No.2, 2008, pp: 192-201

[28] Janison Rodrigues de Carvalho, Carlos A. Duque et al., "A PLL-Based Multirate Structure for Time-Varying Power Systems Harmonic/Interharmonic Estimation", IEEE Transactions on Power Delivery, Vol.24, No.4, 2009, pp: 1789-1800

[29] Sang-Wook Sohn, Young-Bin Lim, Jae-Jun Yun, Hun Choi, and Hyeon-Deok Bae, "A Filter Bank and a Self-Tuning Adaptive Filter for the Harmonic and Interharmonic Estimation in Power Signals", IEEE Transactions on Instrumentation and Measurement, Vol.61, No.1, 2012, pp: 64-73

[30] Hui Xue and Peng Zhang, "Subspace-Least Mean Square Method for Accurate Harmonic and Interharmonic Measurement in Power Systems", IEEE Transactions on Power Delivery, Vol.27, No.3, 2012, pp: 1260-1267

[31] Giovanni Betta, Luigi Ferrigno, and Marco Laracca, "Cost-Effective FPGA Instrument for Harmonic and Interharmonic Monitoring", IEEE Transactions on Instrumentation and Measurement, Vol.62, No.8, 2013, pp: 2161-2170

[32] Cheng-I Chen and Yeong-Chin Chen, "Comparative Study of Harmonic and Interharmonic Estimation Methods for Stationary and Time-Varying Signals", IEEE Transactions on Industrial Electronics, Vol.61, No.1, 2014, pp: 397-404

[33] Zhongmin Sun, Zhengyou He, Tianlei Zang, and Yilu Liu, "Multi-Interharmonic Spectrum Separation and Measurement Under Asynchronous Sampling Condition", IEEE Transactions on Instrumentation and Measurement, Vol.65, No.8, 2016, pp: 1902-1912

[34] M. Hou, "Estimation of Sinusoidal Frequencies and Amplitudes Using Adaptive Identifier and Observer", IEEE Transactions on Automatic Control, Vol.52, No.3, 2007, pp: 493-499

[35] G. Pin, A. Assalone, M. Lovera, and T. Parisini, "Non-asymptotic kernel based parametric estimation of continuous-time linear systems," IEEE Trans. on Automatic Control, vol. 2, no. 61, 2016.